QUASI-TWO DIMENSIONAL FERMI SURFACES IN RARE EARTH AND URANIUM COMPOUNDS: UX_2, $CeTIn_5$ AND $UTGa_5$*

Y. Ōnuki

Graduate School of Science, Osaka University, Toyonaka, Osaka 560-0043, Japan
Advanced Science Research Center, Japan Atomic Energy Research Institute
Tokai, Ibaraki 319-1195, Japan

D. Aoki†, P. Wiśniewski, H. Shishido, S. Ikeda, Y. Inada
R. Settai

Graduate School of Science, Osaka University, Toyonaka, Osaka 560-0043, Japan

Y. Tokiwa, E. Yamamoto, Y. Haga, T. Maehira

Advanced Science Research Center, Japan Atomic Energy Research Institute
Tokai, Ibaraki 319-1195, Japan

H. Harima

The Institute of Scientific and Industrial Research, Osaka University
Ibaraki, Osaka 567-0047, Japan

M. Higuchi

Graduate School of Science, Tohoku University, Sendai, Miyagi 980-8571, Japan

A. Hasegawa

Faculty of Science, Niigata University, Niigata 950-2181, Japan

and H. Yamagami

Faculty of Science, Department of Physics, Kyoto Sangyo University
Kita-ku, Kyoto 603-8555, Japan

(Received June 21, 2001)

We present the quasi-two dimensional Fermi surface studies in rare earth and uranium compounds such as UX_2 (X: Bi, Sb, As and P) and $RTIn_5$ (R: rare earth, T: Co, Rh and Ir), together with $UTGa_5$. The present quasi-two dimensionality is closely related to the magnetic unit cell and/or the unique crystal structure elongated along the tetragonal [001] direction, which bring about a flat Brillouin zone and produce cylindrical but highly corrugated Fermi surfaces along [001].

PACS numbers: 71.18.+y, 71.28.+a

* Presented at the XII School of Modern Physics on Phase Transitions and Critical Phenomena, Lądek Zdrój, Poland, June 21–24, 2001.

† Present address: DRFMC-SPSMS, CEA, 38054 Grenoble Cedex 9, France.

1. Introduction

The f electrons of rare earth and uranium compounds exhibit a variety of characteristics including spin and valence fluctuations, heavy fermions and anisotropic superconductivity [1]. In these compounds, both the Ruderman–Kittel–Kasuya–Yosida (RKKY) interaction and the Kondo effect compete with each other. Competition between the RKKY interaction and the Kondo effect was discussed by Doniach in terms of a function of $|J_{\rm cf}|\,D(\varepsilon_{\rm F})$, where $|J_{\rm cf}|$ is a magnitude of the magnetic exchange interaction and $D(\varepsilon_{\rm F})$ is the electronic density of states at the Fermi energy $\varepsilon_{\rm F}$ [2]. Most of the cerium compounds order magnetically, because the RKKY interaction overcomes the Kondo effect at low temperatures. On the other hand, some cerium compounds such as $CeCu_6$ and $CeRu_2Si_2$ indicate no long-range magnetic order, forming the heavy fermion state at low temperatures.

The heavy fermion state is roughly understood as follows. The $4f$ levels of the Ce ions are generally split into three Crystalline Electric Field (CEF)-doublets at high temperatures because the $4f$ electrons in the Ce compounds are almost localized in nature. At low temperatures, the magnetic entropy of the ground-state doublet in the $4f$ levels, $R\ln 2$, is expressed by integrating the magnetic specific heat $C_{\rm m}$ in the form of $C_{\rm m}/T$ over the temperature. When the magnetic specific heat $C_{\rm m}$ is changed into the electronic specific heat γT via the many-body Kondo effect, the heavy fermion state is formed below the Kondo temperature $T_{\rm K}$: $\gamma = R\ln 2/T_{\rm K} \simeq 10^4/T_{\rm K}({\rm mJ/K^2\,mol})$ [1,3]. In fact, the electronic specific heat coefficient γ and the Kondo temperature are $1600\,{\rm mJ/K^2\,mol}$ and $5\,{\rm K}$ in $CeCu_6$, and $350\,{\rm mJ/K^2\,mol}$ and $20\,{\rm K}$ in $CeRu_2Si_2$, respectively.

The de Haas-van Alphen (dHvA) effect provides a powerful tool for determining the topology of the Fermi surface, the cyclotron effective mass $m_{\rm c}^*$ and the scattering lifetime of the conduction electron. Here, the dHvA voltage $V_{\rm osc}$ is obtained in the so-called 2ω detection of the field modulation method, following the Lifshitz–Kosevich formula: [1]

$$V_{\rm osc} \;=\; A\sin\left(\frac{2\pi F}{H}+\phi\right), \tag{1}$$

$$A \;\propto\; J_2(x)TH^{-1/2}\frac{\exp(-\alpha m_{\rm c}^* T_{\rm D}/H)}{\sinh(\alpha m_{\rm c}^* T/H)}, \tag{2}$$

$$\alpha \;=\; \frac{2\pi^2 c k_{\rm B}}{e\hbar}, \tag{3}$$

and

$$x \;=\; \frac{2\pi F h}{H^2}, \tag{4}$$

where $J_2(x)$ is the Bessel function which depends on the dHvA frequency F,

the modulation field h and the magnetic field strength H. The dHvA frequency F $\left(= \frac{\hbar c}{2\pi e} S_{\mathrm{F}}\right)$ is proportional to the extremal (maximum or minimum) cross-sectional area S_{F} of the Fermi surface and T_{D} $\left(= \frac{\hbar}{2\pi k_{\mathrm{B}}} \tau^{-1}\right)$ is the Dingle temperature which is inversely proportional to the scattering lifetime τ.

Recently quasi-two dimensional Fermi surfaces were observed even in rare earth and uranium compounds. This quasi-two dimensionality is closely related to the magnetic unit cell and/or the crystal structure elongated along the c-axis of the tetragonal or hexagonal crystal structure, which bring about a flat Brillouin zone and produce cylindrical Fermi surfaces along the c-axis. Typical examples are UX_2 (X: Bi, Sb, As, P) [4] and CePtX(X:As, P) [5]. Furthermore, new heavy fermion superconductors of $CeIrIn_5$ and $CeCoIn_5$ or a pressure-induced superconductor of $CeRhIn_5$ with the tetragonal crystal structure are also quasi-two dimensional. We present in this paper quasi-two dimensional Fermi surfaces of UX_2 and $CeTIn_5$ (T: transition atom), together with $UTGa_5$.

2. dHvA studies in quasi-two dimensional compounds

2.1. Cylindrical Fermi surfaces formed by a flat magnetic Brillouin zone in uranium dipnictides

Uranium dipnictides UX_2 (X = Bi, Sb and As) crystallize in the tetragonal structure of anti-Cu_2Sb type (D_{4h}^7 or $P4/nmm$), where the crystal structure of UP_2 is slightly different from that of UX_2 [6]. They order antiferromagnetically. Magnetic moments of uranium ions are aligned ferromagnetically in the (001) planes, which are stacked along the [001] direction in an antiferromagnetic ($\uparrow\downarrow$) sequence in UBi_2 [7]. In the case of USb_2, UAs_2 and UP_2, this sequence is ($\uparrow\downarrow\downarrow\uparrow$) [7–9]. It is worth mentioning here that the magnetic unit cell of USb_2, UAs_2 and UP_2 is doubled with respect to the chemical unit cell along [001], which brings about a flat magnetic Brillouin zone. Here ordered moments and the Néel temperatures are $\mu_{\mathrm{ord}} = 2.1$, 1.88, 1.61 and $2.0\,\mu_{\mathrm{B}}$/U, and $T_{\mathrm{N}} = 183$, 203, 273 and 201 K for X = Bi, Sb, As and P, respectively [10].

First we show the results of the dHvA effect in UBi_2. Figure 1 shows the angular dependence of the dHvA frequency in UBi_2. It follows the $1/\cos\theta$-dependence for the branch β or β' up to 81°. A solid line for these branches in Fig. 1 shows the $1/\cos\theta$-dependence. This result indicates that the branch β or β' originates from a cylindrical but slightly corrugated Fermi surface. In contrast to the branches β and β', the dHvA frequency of the branch α is almost constant against the field angle, meaning that the branch α originates from a nearly spherical Fermi surface. We determined the cyclotron effective

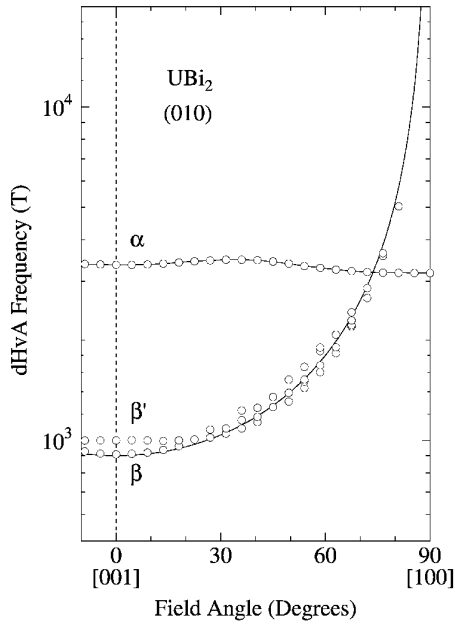

Fig. 1. Angular dependence of the dHvA frequency in UBi_2.

mass m_c^* from the temperature dependence of the dHvA amplitude by using Eq. (2). The cyclotron mass was determined as $9.2\,m_0$ for the branch α, $6.3\,m_0$ for β' and $4.4\,m_0$ for β. The masses are rather large because the corresponding Fermi surfaces have small cross-sections.

Next we show the dHvA results for USb_2. Figure 2 shows the angular dependence of the dHvA frequency in USb_2. It follows the $1/\cos\theta$-dependence for branches α, γ, δ and ε. These results also indicate that branches α, γ, δ and ε originate from cylindrical but slightly corrugated Fermi surfaces. The cyclotron mass was determined as $3.8\,m_0$ for the branch α, $6.0\,m_0$ for γ, $3.8\,m_0$ for δ and $2.0\,m_0$ for ε.

The Fermi surfaces in UBi_2 consist of a cylindrical Fermi surface named β and a spherical one named α. The volume of the cylindrical Fermi surface occupies 4.8 % of the magnetic Brillouin zone, whereas the spherical Fermi surface occupies 9.9 %. As the magnetic unit cell contains two molecules of UBi_2, UBi_2 is a compensated metal with equal carrier numbers of electrons and holes. If we assume that there are one spherical hole-Fermi surface and two cylindrical electron-Fermi surfaces in the Brillouin zone, the number of carriers is well compensated, where the holes and the electrons occupy 9.9 % and 9.6 % of its volume, respectively. We show in Fig. 3 (a) a Brillouin zone and the corresponding Fermi surfaces.

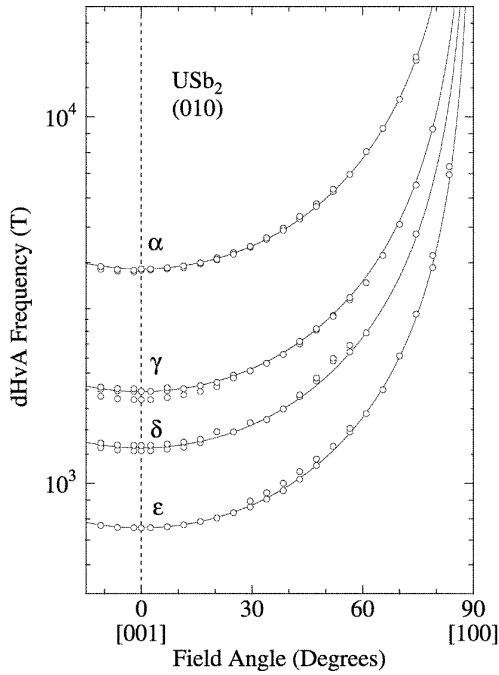

Fig. 2. Angular dependence of the dHvA frequency in USb_2.

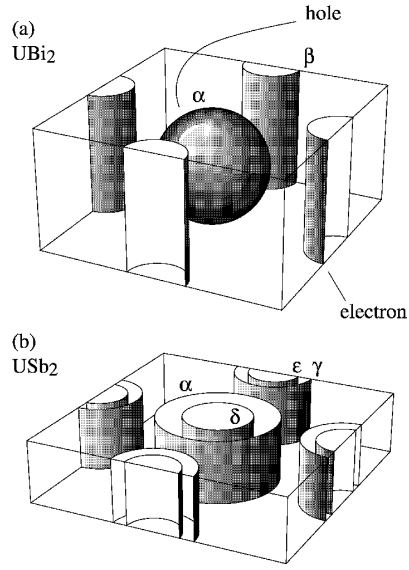

Fig. 3. Schematic magnetic Brillouin zone and the Fermi surfaces (a) for the branches α and β in UBi_2 (b) for the branches α, γ, δ and ε in USb_2.

Furthermore we calculated the γ value from these Fermi surfaces. The estimated γ values from the branches α and β are $\gamma_\alpha = 8.1$ and $\gamma_\beta = 4.9\,\mathrm{mJ/K^2\,mol}$, respectively. The total γ value is thus $\gamma_{m_c^*} = \gamma_\alpha + 2\gamma_\beta = 18\,\mathrm{mJ/K^2\,mol}$, which is in good agreement with $20\,\mathrm{mJ/K^2\,mol}$ determined from the specific heat measurement.

A very flat magnetic Brillouin zone is realized in the antiferromagnetic state of USb_2, although the Brillouin zone in the paramagnetic state is the same as that in UBi_2. It is thus expected that the Fermi surface in USb_2 is approximately the same as that in UBi_2 in the paramagnetic state, although it is modified in the antiferromagnetic state due to the flat magnetic Brillouin zone.

From the angular dependence of the dHvA frequency in Fig. 2, it is seen that all the Fermi surfaces are cylindrical in USb_2. The detected cylindrical Fermi surfaces occupy in the magnetic Brillouin zone 16.8 % for the branch α, 7.9 % for the branch γ, 5.4 % for the branch δ and 3.3 % for the branch ε. As the magnetic unit cell contains four molecules of USb_2, USb_2 is a compensated metal with equal carrier numbers of electrons and holes. To compensate the numbers of the carriers, we assume as follows:

one hole-Fermi surface from the branch α,
one hole-Fermi surface from the branch δ,
two electron-Fermi surfaces from the branch γ and
two electron-Fermi surfaces from the branch ε.

The electron-Fermi surfaces thus occupy 22 % and the hole-Fermi surfaces occupy 22 %, well compensated. Figure 3 (b) shows the flat magnetic Brillouin zone and the corresponding Fermi surfaces in USb_2. The γ value is also consistent with this scheme of the Fermi surfaces.

Experimental results are summarized as follows:

(1) The Fermi surfaces of UBi_2 are found to consist of one spherical Fermi surface and two cylindrical ones.

(2) Each Fermi surface in UBi_2 splits into two cylindrical Fermi surfaces in USb_2, which are well explained by the band-folding procedure in a flat magnetic Brillouin zone.

(3) The quasi-two-dimensional character of these Fermi surfaces is mainly due to the conduction electrons in the U-plane, including the $5f$ electrons because the cyclotron mass is large.

2.2. Quasi-two dimensional Fermi surface originated from the unique tetragonal crystal structure in $RTIn_5$ and $UTGa_5$

$CeRhIn_5$ orders antiferromagnetically below T_N =3.8 K, whereas superconductivity was observed under pressure, p >1.6 GPa [11]. It was also reported that $CeIrIn_5$ and $CeCoIn_5$ are heavy fermion superconductors at ambient pressure [12–15]. The transition temperature T_c and the γ value are 0.4 K and 680 mJ/K^2 mol in $CeIrIn_5$, and 2.3 K and 300-1000 mJ/K^2 mol in $CeCoIn_5$. Here, the γ value in $CeCoIn_5$ is about 300 mJ/K^2 mol at T_c but increases with decreasing the temperature, reaching about 1000 mJ/K^2 mol at 0.1 K, which was obtained by the specific heat measurement in magnetic fields [15].

These characteristic properties in $CeTIn_5$ are closely related to the unique tetragonal crystal structure (P4/mmm #123 D^1_{4h}) with alternating layers of $CeIn_3$ and TIn_2 (T: Co, Rh and Ir), stacked sequentially along the [001] direction (c-axis), as shown in Fig. 4.

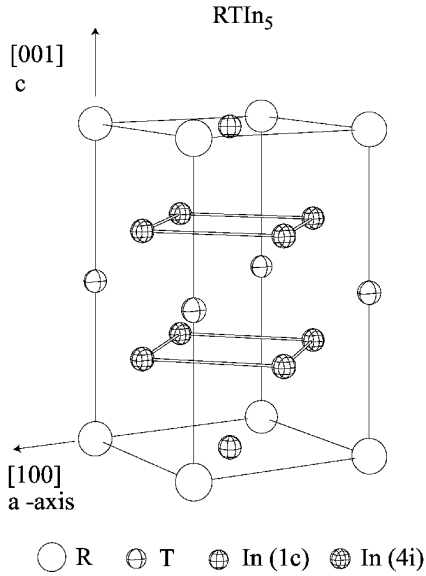

Fig. 4. Tetragonal crystal structure of $RTIn_5$.

First we will show the dHvA experiment for a non-4f reference compound $LaRhIn_5$ [16]. Figure 5(a) shows the angular dependence of the dHvA frequency. The dHvA branches α_i (i=1, 2 and 3) as well as β_2 follow roughly the $1/\cos\theta$-dependence, where θ means a field angle tilted from [001] to [100] or [110]. This angular dependence claims that the corresponding Fermi surface is nearly cylindrical.

Figure 5(b) shows the theoretical dHvA frequency calculated in the scheme of the FLAPW method within the local-density approximation. The magnitude and angular dependence of the dHvA frequency in Fig. 5(a) are the same as theoretical ones in Fig. 5(b), except dHvA branch ε_1.

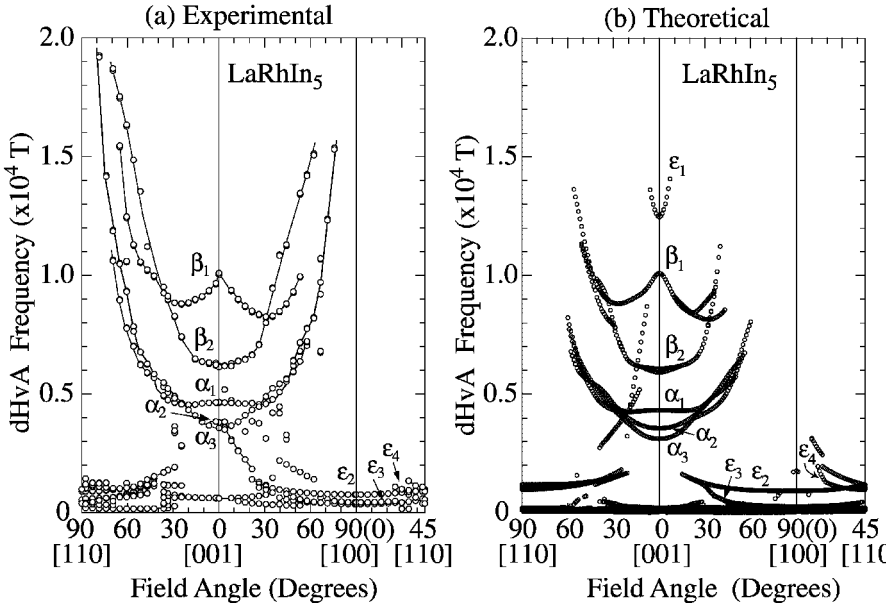

Fig. 5. (a) Angular dependence of the dHvA frequency and (b) the theoretical one in $LaRhIn_5$.

These dHvA branches are well identified by the theoretical Fermi surface in Fig. 6. The dHvA branches α_i are due to a band 15-electron Fermi surface whose topology is nearly cylindrical but is highly corrugated, having maximum and minimum cross-sections. Branches β_i are also due to a highly-corrugated band 14-electron Fermi surface. This Fermi surface has a convex part stretching along the [110] direction. This is a main reason why the dHvA frequency of branch β_1 has a minimum at about $\theta = 30°$, tilted from [001] to [100] or [110]. Branches ε_i are due to a band 13-hole Fermi surface, forming a network or a lattice. The orbit ε_1 in Fig. 6(a) was, however, not detected experimentally, which is most likely due to the damping of the dHvA amplitude based on a curvature factor of this Fermi surface.

Next, the dHvA experiment for $CeRhIn_5$ was carried out in the antiferromagnetic state [16,17]. Figure 7 shows the angular dependence of the dHvA frequency. Main three branches are named β_2, α_1, and α_3. To identify these branches, we compare them to those of $LaRhIn_5$ and $CeCoIn_5$, as shown in Fig. 8. If the $4f$ electrons in $CeRhIn_5$ are localized and the Fermi surface

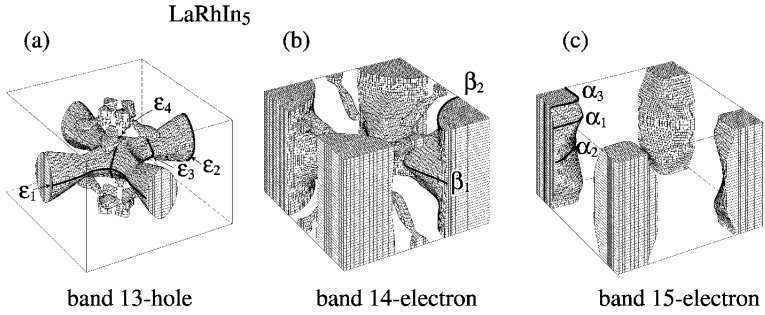

Fig. 6. Theoretical (a) band 13-hole, (b) band 14-electron and (c) band 15-electron Fermi surfaces in $LaRhIn_5$.

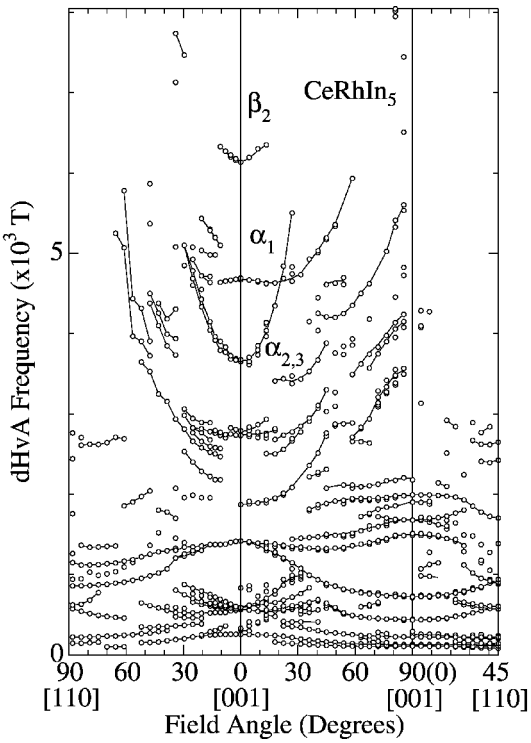

Fig. 7. Angular dependence of the dHvA frequency in $CeRhIn_5$.

is not affected by the small magnetic Brillouin zone, the Fermi surface in $CeRhIn_5$ should be the same as that of $LaRhIn_5$. On the other hand, if the $4f$ electrons are itinerant as in $CeIrIn_5$ and $CeCoIn_5$, the Fermi surface of $CeRhIn_5$ should be the same as that of $CeCoIn_5$. Note that the topology of the Fermi surface is approximately the same between $CeIrIn_5$ and $CeCoIn_5$, which were well explained by the $4f$-itinerant model as shown below [18,19].

A dHvA frequency with F=6.13 $\times 10^3$ T of branch β_2 in $CeRhIn_5$ is the same as 6.13 $\times 10^3$ T in $LaRhIn_3$, but is smaller than 7.35 $\times 10^3$ T in $CeCoIn_5$. The dHvA frequencies of branches α_1 and $\alpha_{2,3}$ in $CeRhIn_5$ are also the same as those of $LaRhIn_5$, but are smaller than those of $CeCoIn_5$, as shown in Fig. 8.

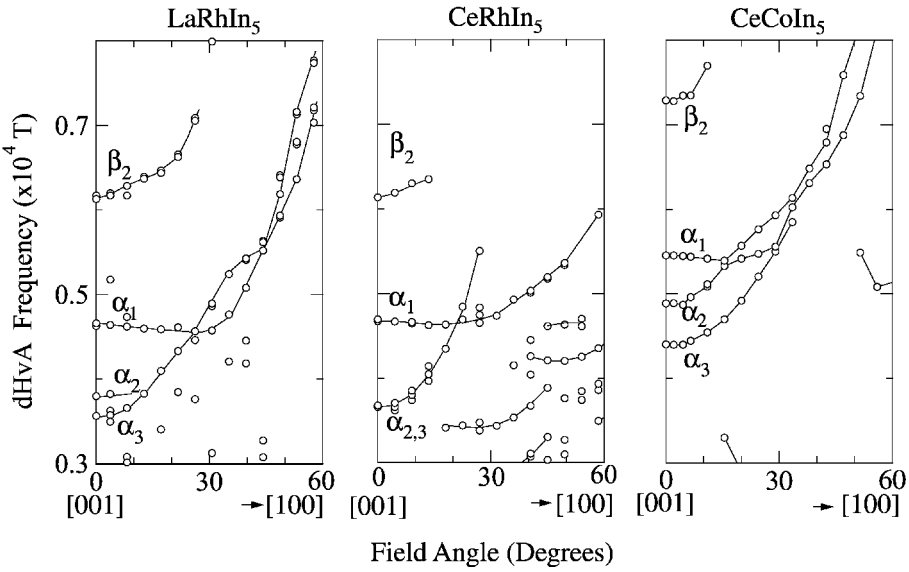

Fig. 8. Angular dependence of main dHvA frequencies in (a) $LaRhIn_5$, (b) $CeRhIn_5$ and (c) $CeCoIn_5$.

From these experimental results we can conclude that the contribution of the $4f$ electrons to the volume of the Fermi surface in $CeRhIn_5$ is negligibly small. We note that there are so many dHvA branches in $CeRhIn_5$ compared to those in $LaRhIn_5$. This might be approximated by a band-folding procedure where the paramagnetic Fermi surface of $CeRhIn_5$, which is almost the same as that of $LaRhIn_5$, is folded into a small magnetic Brillouin zone based on a large magnetic unit cell, producing small Fermi surfaces. Branches β_2, α_1 and $\alpha_{2,3}$ are most likely formed by the conduction electrons which break through the antiferromagnetic Brillouin zone boundary and circulate around the original paramagnetic Fermi surface and/or some of these branches are not affected by the magnetic Brillouin zone.

On the other hand, the cyclotron effective mass of $CeRhIn_5$ is large compared to that of $LaRhIn_5$. The cyclotron mass is 5.5 m_0 in branch β_2, 6.0 m_0 in branch α_1 and 3.5 m_0 in branch $\alpha_{2,3}$. The corresponding mass in $LaRhIn_5$ is 0.73 m_0, 0.69 m_0 and 0.51&0.64 m_0, respectively. The ratio of the mass of $CeRhIn_5$ to that of $LaRhIn_5$ is about 7–9. On the other hand, the

ratio of the γ value of $CeRhIn_5$ to that of $LaRhIn_5$ is about 9, where $\gamma \simeq 50$ mJ/K^2 mol in $CeRhIn_5$ and 5.7 mJ/K^2 mol in $LaRhIn_5$. Both ratios are approximately consistent. These experimental results are almost the same as the recent results in $CeRhIn_5$ [20,21]. For example, main branches β_2 and $\alpha_{2,3}$ were observed: F=6.120×10^3 T (m_c^*=6.1±0.3 m_0) and F=3.600×10^3 T (m_c^*=4.6±1.0 m_0), respectively.

We would like to clarify the $4f$-electronic nature in $CeCoIn_5$. Figure 9 shows the angular dependence of dHvA frequency in $CeCoIn_5$. The dHvA branches in Fig. 9(a) are well identified by the $4f$-itinerant band model, where Figure 9(b) shows the angular dependence of the theoretical dHvA frequency in $CeCoIn_5$. Main branches α_i and β_i in Fig. 9 are identified by theoretical Fermi surfaces in Fig. 10.

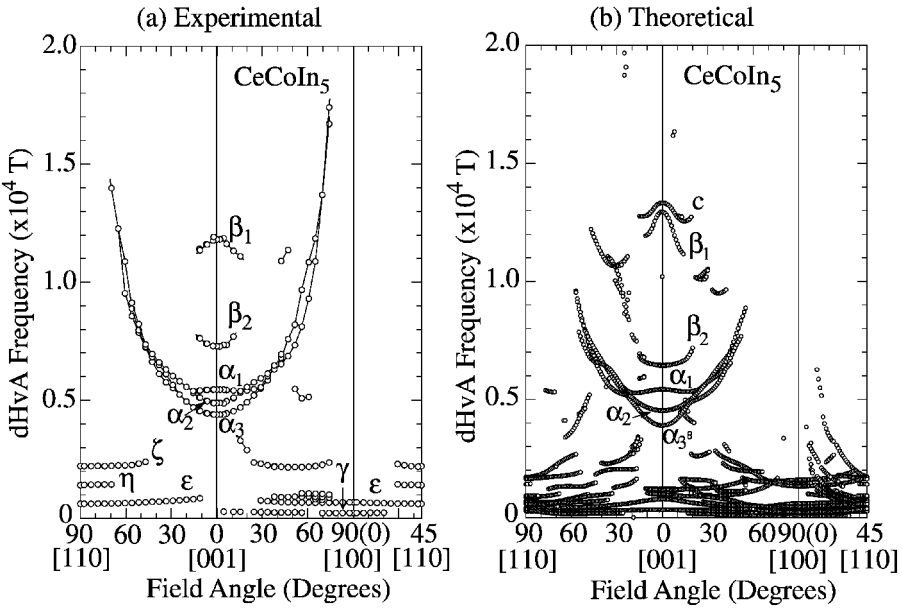

Fig. 9. (a) Angular dependence of the dHvA frequency and (b) the theoretical one in $CeCoIn_5$.

Fermi surfaces in $CeCoIn_5$ are similar to those of $LaRhIn_5$, although the size of each Fermi surface is different between them. A similar relation is present between the Fermi surface of Pb with four valence electrons and that of Al with three valance electrons. If one $4f$-electron in each Ce site becomes a conduction electron in $CeCoIn_5$, the volume of the band 13-hole Fermi surface in $LaRhIn_5$, shown in Fig. 6(a), is shrunken, changing into two kinds of small closed Fermi surfaces in $CeCoIn_5$, as shown in Fig. 10(a). Correspondingly, the band 14- and 15-electron Fermi surfaces are expanded

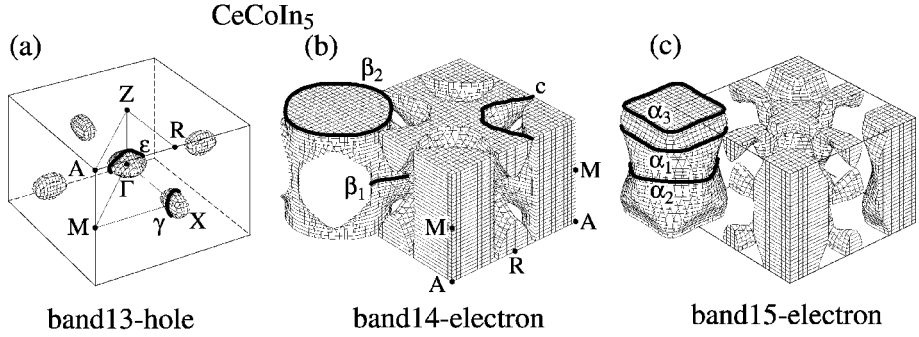

Fig. 10. Theoretical Fermi surfaces in $CeCoIn_5$.

in volume. The band 14- and 15-electron Fermi surfaces in Fig. 6(b) and (c) are changed into Fermi surfaces in Fig. 10(b) and (c), respectively. This is a reason why the dHvA frequencies of β_i and α_i in $CeCoIn_5$ are larger than those in $LaRhIn_5$.

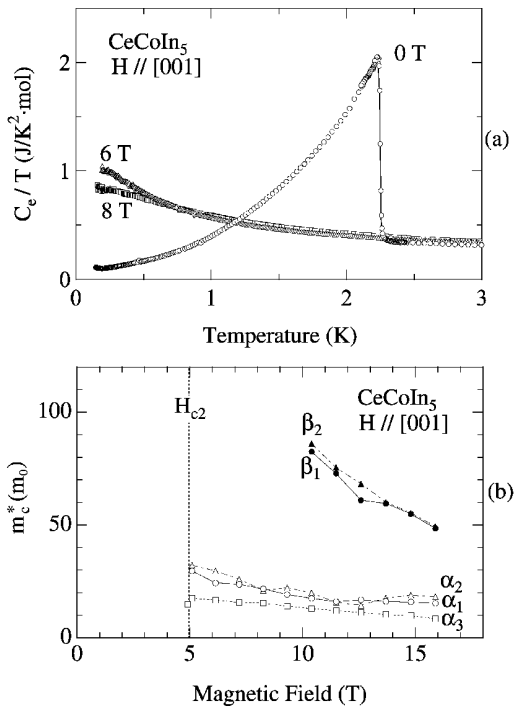

Fig. 11. (a) Temperature dependence of the specific heat C_e in the form of C_e/T under H=0, 6 and 8 T. (b) Field dependence of the cyclotron mass in $CeCoIn_5$.

As shown in Fig. 11, the cyclotron mass of $CeCoIn_5$ is extremely large. For example, the mass of β_i is about 80 m_0 at 10 T. The cyclotron mass is strongly field-dependent, where $80\,m_0$ at 10 T is reduced to $50\,m_0$ at 16 T for branch β_i [19]. A large cyclotron mass over $100\,m_0$ is expected at lower fields than 10 T, consistent with the specific heat coefficient in magnetic fields. Similar dHvA results are obtained in $CeIrIn_5$ [18].

$UTGa_5$ (T: transition atom) has also the $HoCoGa_5$-type tetragonal crystal structure as in $RTIn_5$. Here we present dHvA results in a series of $UTGa_5$, namely Pauli paramagnets of $UFeGa_5$ and $UCoGa_5$, and an antiferromagnet $UPtGa_5$.

We show in Fig. 12(a) the angular dependence of the dHvA frequency in $UFeGa_5$ [22], together with the theoretical one in Fig. 12(b). Branches α_i show roughly a $1/\cos\theta$-dependence of the dHvA frequency. Branches b_i are disconnected in the angular dependence, indicating a multiply-connected Fermi surface. The origin of these detected dHvA branches is well explained on the basis of the theoretical Fermi surfaces in Fig. 13. Namely, branches α_i are due to a highly corrugated but cylindrical Fermi surface, and a_i and b_i are due to a lattice like structure in the band 15.

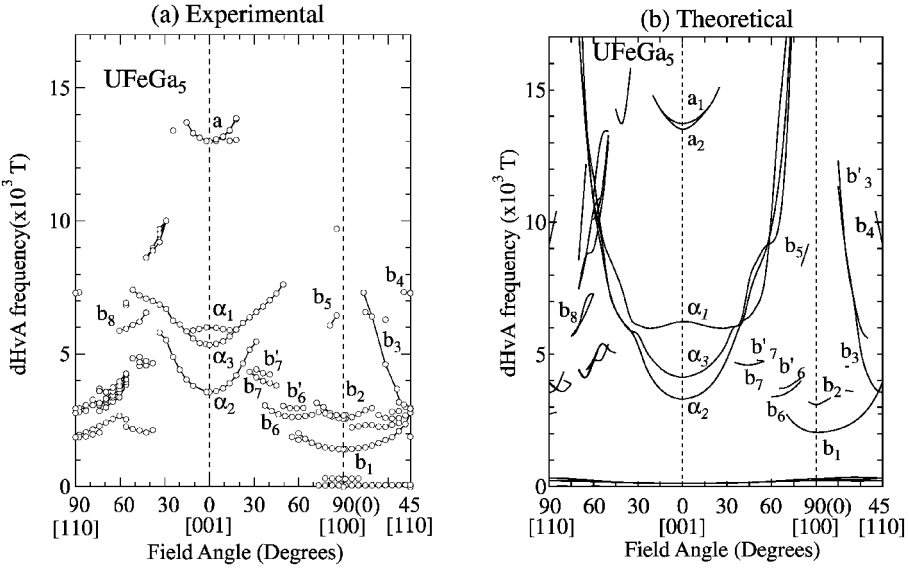

Fig. 12. Angular dependence of the (a) dHvA frequency and (b) the theoretical one in $UFeGa_5$.

We will compare the Fermi surface of $UFeGa_5$ with valence electrons of $U(5f^3 6d^1 7s^2)$, $Fe(3d^6 4s^2)$ and $Ga(4s^2 4p^1)$ to that of $CeCoIn_5$ with valence electrons of $Ce(4f^1 5d^1 6s^2)$, $Co(3d^7 4s^2)$ and $In(5s^2 5p^1)$. $CeCoIn_5$ is a compensated metal with equal volumes of electron- and hole-Fermi sur-

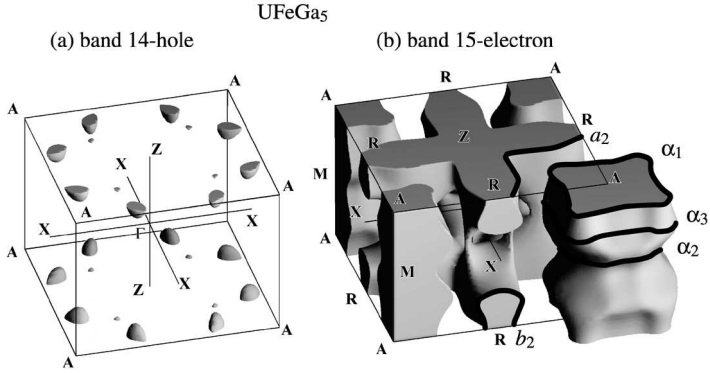

Fig. 13. Fermi surface of (a) band 14-holes, (b) band 15-electrons in $UFeGa_5$.

faces. If the band 14-hole Fermi surface in $CeCoIn_5$ is almost fully occupied by an electron and also the volume of the band 15-electron Fermi surface is slightly enlarged, these Fermi surfaces correspond to the band 14-small hole Fermi surfaces and the band 15-large electron ones, respectively, in $UFeGa_5$. In $CeCoIn_5$ we could not observe the lattice-structure like band 15-electron Fermi surface, while the corresponding Fermi surface was detected completely in $UFeGa_5$. We suppose that the lattice-structure like band 15-Fermi surface is not present and/or is changed into small closed Fermi surfaces in $CeCoIn_5$.

The $5f$ electrons in $UFeGa_5$ are highly itinerant compared to the $4f$ electrons in $CeCoIn_5$. The cyclotron mass in $UFeGa_5$ is relatively large: 9.2, 4.6 and 8.0 m_0 for α_i (i=1, 2 and 3), respectively.

In $UCoGa_5$ we observed dHvA branches with small dHvA frequencies, as shown in Fig. 14. This means that $UCoGa_5$ is a semimetal. The Fermi surface most likely consists of small band 15-hole Fermi surfaces and small band 16-electron Fermi surfaces, because one more valence electron is added, compared to that in $UFeGa_5$. In fact, a volume of one ellipsoidal Fermi surface (branch a) is equal to a volume of two pieces of ellipsoidal Fermi surfaces (branch b) and four pieces of ellipsoidal Fermi surfaces (branch c): $V_a = 2V_b + 4V_c$ (V_a=0.0059 $V_{\rm BZ}$, V_b=0.0019 $V_{\rm BZ}$ and V_c=0.0005 $V_{\rm BZ}$), where $V_{\rm BZ}$ is a volume of the Brillouin zone.

Finally we show in Fig. 15 the angular dependence of the dHvA frequency in an antiferromagnet $UPtGa_5$ with $T_{\rm N}$=25 K and an ordered moment of 0.25 $\mu_{\rm B}$/U. Most of the dHvA branches indicate the $1/\cos\theta$-dependence, claiming cylindrical Fermi surfaces. The magnetic unit cell of $UPtGa_5$ is doubled with respect to the chemical unit cell along [001], which brings about a flat magnetic Brillouin zone as in USb_2. This is a main reason on the existence of the cylindrical Fermi surfaces in $UPtGa_5$. The cyclotron mass is in the range of 10 to 25 m_0 for [001], reflecting the γ value of 57 mJ/K^2 mol.

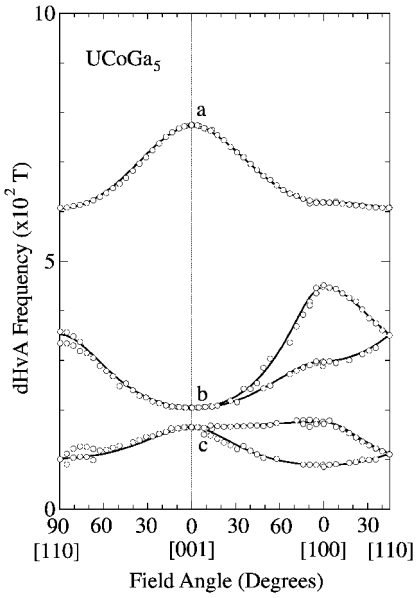

Fig. 14. Angular dependence of the dHvA frequency in $UCoGa_5$.

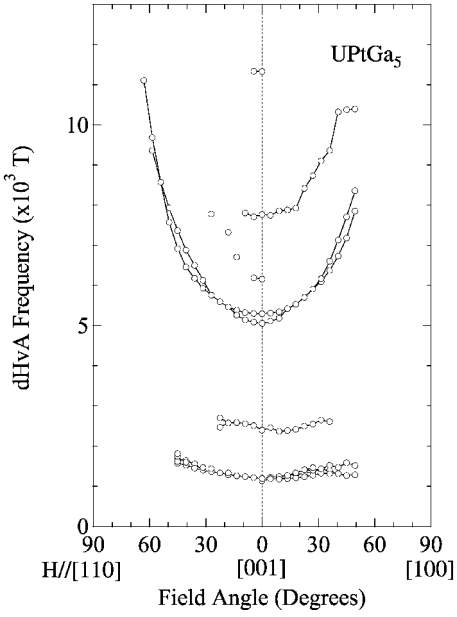

Fig. 15. Angular dependence of the dHvA frequency in $UPtGa_5$.

3. Concluding remark

High-quality single crystals, low temperatures and strong magnetic fields are fundamentally necessary to demonstrate the dHvA measurement for the strongly correlated electron systems. At present, the carrier with a large cyclotron mass over $100\,m_0$ is detected in the dHvA experiment for $CeRu_2Si_2$, UPt_3 and $CeCoIn_5$, reflecting the γ value of $57\,mJ/K^2$ mol.

Quasi-two dimensionality in rare earth and uranium compounds is closely related to the magnetic unit cell and/or the unique crystal structure as well as the corresponding electronic state. In UX_2, the conduction electrons are $5f$, $6d$ and $7s$ electrons in the U-plane. It is expected that these conductive U-planes are separated by the nearly non-conductive X-planes, bringing about the quasi-two dimensional electronic state. The magnetic unit cell, doubled with respect to the chemical unit cell along [001], enhances two dimensionality because the unit length along [001] in the Brillouin zone becomes half and correspondingly each Fermi surface is band-folded in the flat Brillouin zone.

The similar quasi-two dimensionality is also realized in the unique tetragonal crystal structure of $RTIn_5$ and $UTGa_5$. It was demonstrated that the topology of the Fermi surface in $UFeGa_5$ is well explained by the $5f$-itinerant band model, compared to that in $CeCoIn_5$. This indicates that the $5f$ electrons are itinerant as the $3d$ electrons, while the $4f$ electrons become itinerant via the many-body Kondo effect at low temperatures. A different mechanism between them results in a different cyclotron effective mass between them.

The present work was financially supported by a Grant-in-Aid for Scientific Research COE(10CE2004) and a Grant-in-Aid for Scientific Research from the Ministry of Education, Science, Sports and Culture.

REFERENCES

[1] Y. Ōnuki, T. Goto, T. Kasuya, *Mater. Sci. Technol.*, Vol. 3A, Chap. 7, ed. K.H.J. Buschow VCH, Weinheim 1991, p. 545.

[2] S. Doniach, *Physica* **B91**, 231 (1977).

[3] Y. Ōnuki, Y. Inada, H. Ohkuni, R. Settai, N. Kimura, H. Aoki, Y. Haga, E. Yamamoto, *Physica* **B280**, 276 (2000).

[4] D. Aoki, P. Wiśniewski, K. Miyake, N. Watanabe, Y. Inada, R. Settai, E. Yamamoto, Y. Haga, Y. Ōnuki, *Philos. Mag.* **B80**, 1517 (2000).

[5] R. Settai, Y. Yoshida, A. Yamaguchi, Y. Ōnuki, S. Yoshii, M. Kasaya, H. Harima, K. Takegahara, *J. Phys. Soc. Jpn.* **68**, 3615 (1999).

[6] P. Wiśniewski, D. Aoki, N. Watanabe, R. Settai, Y. Haga, E. Yamamoto, Y. Ōnuki, *J. Phys. Soc. Jpn.* **70**, 278 (2001).

[7] J. Leciejewicz, R. Troć, A. Murasik, A. Zygmunt, *Phys. Status Solidi* **22**, 517 (1967).

[8] R. Troć, J. Leciejewicz, R. Ciszewski, *Phys. Status Solidi* **15**, 515 (1966).

[9] A. Oleś, *J. Phys.* **26**, 561 (1965).

[10] G. Amoretti, A. Blaise, J. Mulak, *J. Magn. Magn. Mater.* **42**, 65 (1984).

[11] H. Hegger, C. Petrovic, E.G. Moshopoulou, M.F. Hundley, J.L. Sarrao, Z. Fisk, J.D. Thompson, *Phys. Rev. Lett.* **84**, 4986 (2000).

[12] J.D. Thompson, R. Movshovich, N.J. Curro, P.C. Hammel, M.F. Hundley, M. Jaime, P.G. Pagliuso, J.L. Sarrao, C. Petrovic, Z. Fisk, F. Bouquet, R.A. Fisher, printed in *J. Magn. Magn. Mater.* (ICM'2000, Recife, Brazil).

[13] R. Movshovich, M. Jaime, J.D. Thompson, C. Petrovic, Z. Fisk, P.G. Pagliuso, J.L. Sarrao, *Phys. Rev. Lett.* **86**, 5152 (2001).

[14] C. Petrovic, R. Movshovich, M. Jaime, P.G. Pagliuso, M.F. Hundley, J.L. Sarrao, Z. Fisk, J.D. Thompson, *Europhys. Lett.* **53**, 354 (2001).

[15] C. Petrovic, P.G. Pagliuso, M.F. Hundley, R. Movshovich, J.L. Sarrao, J.D. Thompson, Z. Fisk, P. Monthoux, *J. Phys.: Condens. Matter* **13**, L337 (2001).

[16] H. Shishido, R. Settai, D. Aoki, S. Ikeda, N. Nakamura, T. Iizuka, Y. Inada, K. Sugiyama, T. Takeuchi, K. Kindo, Y. Haga, H. Harima, Y. Aoki, T. Namiki, H. Sato, Y. Ōnuki, submitted to *J. Phys. Soc. Jpn.*

[17] T. Takeuchi, T. Inoue, K. Sugiyama, D. Aoki, Y. Tokiwa, Y. Haga, K. Kindo, Y. Ōnuki, *J. Phys. Soc. Jpn.* **70**, 877 (2001).

[18] Y. Haga, Y. Inada, H. Harima, K. Oikawa, M. Murakawa, H. Nakawaki, Y. Tokiwa, D. Aoki, H. Shishido, S. Ikeda, N. Watanabe, Y. Ōnuki, *Phys. Rev.* **B63**, 060503(R) (2001).

[19] R. Settai, H. Shishido, S. Ikeda, Y. Murakawa, M. Nakashima, D. Aoki, Y. Haga, H. Harima, Y. Ōnuki, *J. Phys.: Condens. Matter* **13**, L627 (2001).

[20] A.L. Cornelius, A.J. Arko, J.L. Sarrao, M.F. Hundley, Z. Fisk, *Phys. Rev.* **B62**, R14181 (2000).

[21] D. Hall, E. Palm, T. Murphy, S. Tozer, E. Miller-Ricci, L. Peabody, C.Q.H. Li, U. Alver, R.G. Goodrich, J.L. Sarrao, P.G. Pagliuso, J.M. Wills, Z. Fisk, preprint.

[22] Y. Tokiwa, T. Maehira, S. Ikeda, Y. Haga, E. Yamamoto, A. Nakamura Y. Ōnuki, M. Higuchi, A. Hasegawa, submitted to *J. Phys. Soc. Jpn.*